Journal of Photochemistry, 19 (1982) 189 - 207

ABSORPTION COEFFICIENTS AND KINETICS OF THE BrO RADICAL USING MOLECULAR MODULATION

R. A. COX and D. W. SHEPPARD†

Environmental and Medical Sciences Division, Atomic Energy Research Establishment, Harwell, Oxon. OX11 0RA (Gt. Britain)

M. P. STEVENS

Instrumentation and Applied Physics Division, Atomic Energy Research Establishment, Harwell, Oxon, OX11 0RA (Gt. Britain)

(Received November 30, 1981; in revised form January 28, 1982)

Summary

BrO radicals were produced by square-wave-modulated photolysis of Br_2–O_3 mixtures and detected in absorption by molecular modulation spectrometry. The spectrum of BrO in the region 296 - 375 nm has been determined from absorption measurements at 0.1 nm intervals and with 0.22 nm resolution. A total of 17 bands in the A $^2\Pi \leftarrow$ X $^2\Pi$ system were observed and the absorbance in these bands was put on an absolute basis by measurement of the cross section for absorption at the band head of the $(v' = 7) \leftarrow (v'' = 0)$ transition at 338.3 nm.

Kinetic studies of BrO in the modulated photolysis system yielded a rate constant for the reaction

$$BrO + BrO \xrightarrow{k_5} Br_2 + O_2$$

where $k_5 = (6.6 \pm 1.5) \times 10^{-13}$ cm^3 molecule^{-1} s^{-1}. k_5 showed no significant temperature dependence over the range 278 - 338 K.

1. Introduction

In common with the other halogen oxide species, BrO possesses a characteristic banded spectrum in the near-UV which is due to the A $^2\Pi \leftarrow$ X $^2\Pi$ electronic transition. Durie and Ramsay [1] were the first to investigate the spectrum in absorption using flash photolysis of Br_2–O_2 mixtures to generate BrO. Subsequently absorption in these bands has been used to

†Present address: Department of Chemistry, University of Nottingham, Gt. Britain.

0047-2670/82/0000-0000/$02.75

monitor BrO in several kinetics studies of this radical using techniques of flash photolysis [2 - 4] and discharge flow [5, 6].

The reactions of BrO are currently of interest from the point of view of atmospheric chemistry since Br and BrO are active catalysts for the destruction of ozone in the stratosphere through reactions such as

$$Br + O_3 \rightarrow BrO + O_2 \quad (1)$$

$$O + BrO \rightarrow Br + O_2 \quad (2)$$

The bromine-containing species in the stratosphere originate from the photochemically initiated oxidation of trace bromine compounds, *e.g.* CH_3Br, $C_2H_4Br_2$ and CF_3Br, which are released into the atmosphere from man-made sources [7]. In contrast with stratospheric chlorine which is mostly present as HCl, bromine in the stratosphere is predominantly in the form of reactive BrO since HBr is less readily formed by the reaction of Br with hydrogen-containing species and is also more reactive than HCl towards OH and photochemical destruction [8]. The spectrum of BrO is also of interest for atmospheric chemistry since unlike ClO the absorption extends into the near-UV region which is present in sunlight at all altitudes. BrO exhibits extensive predissociation following absorption in the above electronic transition [1] and therefore photodissociation is a potentially important feature of the behaviour of BrO in the atmosphere:

$$BrO + h\nu \rightarrow Br + O \quad (3)$$

Evaluation of the photodissociation rate requires a detailed knowledge of the absolute absorption cross sections for BrO measured at sufficiently high resolution so that the overlap envelope of the vibronic bands with the solar spectrum can be accurately determined.

There have been several quantitative determinations of the absorption cross section for BrO in the 7–0 band at $\lambda = 338.3$ nm [2, 4, 5]. Although the magnitude of the cross section σ is dependent upon instrumental parameters such as the spectral bandwidth, it is probable that the substantial variation in the reported values of σ cannot be entirely attributed to this cause. Consequently there is no reliable absolute value of σ which can be used for the computation of atmospheric photolysis rates. Furthermore the spectral information reported both in the high resolution study [1] and the other studies [3 - 6] is not presented in sufficient quantitative detail for accurate determination of the cross sections at other wavelengths relative to that in the 7–0 band.

The uncertainty in the absorption cross section also affects kinetic measurements when UV absorption is employed to monitor BrO. This applies particularly to reactions that are second order in BrO concentration, *e.g.*

$$BrO + BrO \rightarrow 2Br + O_2 \quad (4)$$

$$\rightarrow Br_2 + O_2 \quad (5)$$

where there are substantial variations in the reported values for the overall

rate coefficient $k_4 + k_5$ and in its temperature dependence [3 - 5]. Some of the differences may arise from differences in σ.

Although it has been widely believed that reaction (4), producing atomic bromine, is the major channel in BrO disproportionation, there has only been one very recent study in which the branching ratio was determined directly [4]. This study gave $k_4/(k_4 + k_5) = 0.84 \pm 0.03$ at 298 K which is consistent with independent observations of the quantum yields for Br_2-photosensitized decomposition of O_3 [9]. The temperature dependences of k_5 and k_4 in isolation have not been measured.

In the present work the molecular modulation technique has been used to study the UV spectrum and kinetics of BrO in the photolysis of Br_2–O_3 mixtures. The spectrum was obtained from observation of modulated absorption with a resolution of 0.22 nm over the range 295 - 375 nm and the rate coefficient k_5 was determined from time-resolved observation of BrO absorption during the square wave photolysis cycle. Absolute values of σ were obtained from the kinetic measurements together with the measured photochemical BrO production rate. The quantum yield for the Br_2-photosensitized decomposition of O_3 was also determined and used to obtain an estimate of k_4.

2. Experimental details

The molecular modulation spectrometer has been described before [10]. In the present work major modifications were made to the signal processing arrangements and these are described in some detail below. The jacketed quartz reaction cell was 86 cm long and 2.5 cm in diameter. Two different actinic lamps were used for photolysis: O_3 photolysis was conducted using 254 nm radiation from up to three low pressure mercury lamps (Philips TUV/30), and Br_2 photolysis was conducted using broad band visible radiation (375 - 750 nm) from up to three standard "white" fluorescent lamps (Thorn 40 W). The spectral monitoring light from a deuterium lamp (Manufacturers Supply Ltd.) passed axially through the cell and was dispersed on a 0.75 m Czerny–Turner monochromator (Spex, model 1700, reciprocal dispersion 0.11 nm mm^{-1}).

In previous work the modulated absorption was detected using a digital lock-in system. Signal output was in the form of in-phase and in-quadrature absorption components obtained by integrating the digitized signal in reversible counters timed to operate synchronously with the photolysis lamps. By accumulating signals over a large number of successive photolysis cycles, random noise is averaged out and small phase-related absorptions of the order of 10^{-4} can be detected. Whilst this system is ideal for the detection of relative absorptions, such as is required for spectra of transient species, kinetic information which is contained in the phase shift of the absorption relative to the photolysis lamps is more difficult to extract, particularly for systems exhibiting complex kinetics when the chemistry

controlling the radical concentration in the light and dark periods differs. The difficulty arises because the net signal results from integration over light and dark periods, followed by subtraction of the integrated signals. In this way the time base and hence the detailed kinetic information present during each half-cycle is lost. The time base is then obtained by repeating experiments over a range of photolysis frequencies.

An alternative method of collecting and averaging the time-dependent absorption signal uses a multichannel analyser. In this way the whole waveform for time dependence of absorption in a cycle can be detected, with a corresponding increase in information gained and ease of interpretation. The loss of signal averaging commensurate with the gain in time resolution can be easily offset by using longer averaging times. Modifications were made to the existing equipment to provide multichannel detection of the modulated absorption using an internally preprogrammed microcomputer (Harwell MOUSE type 6161) controlled externally by a CBM PET 3022. A schematic diagram of the system is given in Fig. 1.

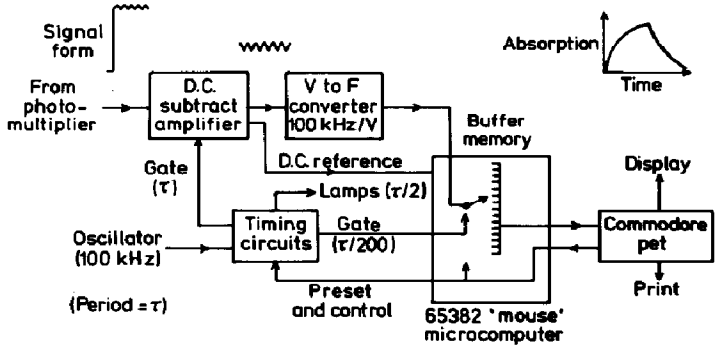

Fig. 1. Schematic diagram of the multichannel waveform analyser.

The signal from the photomultiplier containing the modulated absorption was fed as before to a differencing amplifier to remove the carrier d.c., amplified by a factor of 50 and fed to a voltage-to-frequency converter (ANCOM 15 VF-1, 100 kHz V^{-1}). The digitized signal was then fed alternately to two scalers in MOUSE which were gated with a channel width of $\tau/200$ (τ is the photolysis period). The contents of one scaler were transferred to a 200-channel buffer memory whilst the second scaler accumulated the signal for the next channel. The reference d.c. signal for each cycle was also digitized and fed to a separate register. The operation was defined in a programmable read-only memory internal to MOUSE and the requisite timing signals for the photolysis lamp driver and for controlling the scalers were obtained from modulo-N counters operating on the output from a 100 kHz crystal-controlled oscillator.

The minimum gating time of the multichannel analyser, determined by the speed of the control instructions in MOUSE, was 1 ms per channel giving a maximum operating modulation frequency of 5 Hz.

The selected period and total experiment time were entered from the PET keyboard. At the end of an experiment the contents of the 200-channel memory were transferred to the PET and displayed. Data from more experiments could then be added until the required amount of signal averaging was achieved. Typically the noise level in a single channel was 2×10^{-4} absorption units from a 300 s averaging time. The resulting waveform was then processed on line to provide absorption–time data for the absorbing species during the photolysis cycle. The in-phase and in-quadrature components could be calculated at this stage if required. Calibration was effected by feeding a square wave of amplitude 1 mV and a 1 V reference d.c. into the detector.

The experiments were performed using gas mixtures prepared by mixing flows in a manifold at atmospheric pressure. A bromine flow of 3×10^{16} molecules s^{-1} was obtained by passing nitrogen (BOC, high purity) through bromine (BDH AnalaR grade) contained in a trap at −78 °C. An ozone flow of up to 8×10^{16} molecules s^{-1} was obtained by passing pure oxygen (BOC Breathing grade) through a small silent-discharge ozonizer. Additional oxygen and nitrogen were added to obtain the required composition. Formaldehyde (approximately 2×10^{17} molecules s^{-1}) was obtained by passing nitrogen diluent over paraformaldehyde heated to 70 °C.

For BrO absorption measurements the gas mixtures flowed through the 829 cm^3 reaction cell at flow rates between 1.2 and 2.5 l min^{-1} at 1 atm pressure. Measurements of the Br_2 and O_3 reaction rates were conducted in the stopped-flow mode, *i.e.* on static reaction mixtures.

3. Results

3.1. Absorption spectrum of BrO

The spectrum originating from the $A\ ^2\Pi \leftarrow X\ ^2\Pi$ electronic transition of BrO was obtained from measurement of the in-phase and in-quadrature components of modulated absorption in the range 297 - 375 nm resulting from the 0.3 Hz modulated photolysis at 254 nm of O_3–Br_2–O_2 mixtures in nitrogen diluent at 1 atm pressure and 303 K. In this system BrO is produced and removed by the following reactions:

$$O_3 + h\nu \rightarrow O(^1D) + O_2(^1\Delta) \quad (6)$$

$$O(^1D) + M \rightarrow O(^3P) + M \qquad (M \equiv N_2, O_2) \quad (7)$$

$$O_2(^1\Delta) + O_3 \rightarrow O(^3P) + 2O_2 \quad (8)$$

$$O(^3P) + Br_2 \rightarrow Br + BrO \quad (9)$$

$$Br + O_3 \rightarrow BrO + O_2 \quad (1)$$

$$BrO + BrO \rightarrow 2Br + O_2 \quad (4)$$

$$\rightarrow Br_2 + O_2 \quad (5)$$

The mixture composition was 3.0×10^{15} molecules O_3 cm^{-3}, 2.1×10^{14} molecules Br_2 cm^{-3} and 1.1×10^{18} molecules O_2 cm^{-3}. The ratio $[Br_2]/[O_2]$ was chosen so that about 75% of the $O(^3P)$ atoms produced as a result of O_3 photolysis recombined with O_2 to re-form O_3:

$$O(^3P) + O_2 + M \rightarrow O_3 + M \qquad (10)$$

This ensured that O_3, which is removed both by photolysis and by reaction with Br and $O_2(^1\Delta)$, was not depleted by more than 50% during the residence time in the cell (21 s).

The absorption measurements were made under steady state flow conditions with a photolysis period of 3 s and an averaging time of 30 s. This gave a minimum detectable absorption of about 5×10^{-5}, corresponding to a signal-to-noise ratio of about 50 for the measurements of in-phase absorption near the band maxima. The spectral slit width for the measurements was 0.22 nm; an increase in resolution to 0.11 nm led to no significant increase in the apparent absorption in the bands showing that the vibrational features were adequately resolved in this configuration. Rotational fine structure was not resolved, however. Measurements were made in the 297 - 375 nm range, mostly at 0.1 nm intervals.

Figure 2 shows the observed spectrum which consists of 17 vibronic bands in a progression from 361 nm where the first clearly defined band occurs to 297.6 nm. The spacing between the band heads is about 6 nm at the long wavelength end decreasing to 2.5 nm at the shorter wavelengths. The strongest band head occurs at 338.3 nm and in this region the bands are superimposed on a weak continuum. The features of the spectrum and the positions of the band heads are in excellent agreement with previous observations of this spectrum. Recently Ramsay and coworkers [11] have observed additional weak bands at longer wavelengths and have reassigned the vibronic transitions in this progression. The maximum at 338.3 nm is now assigned to

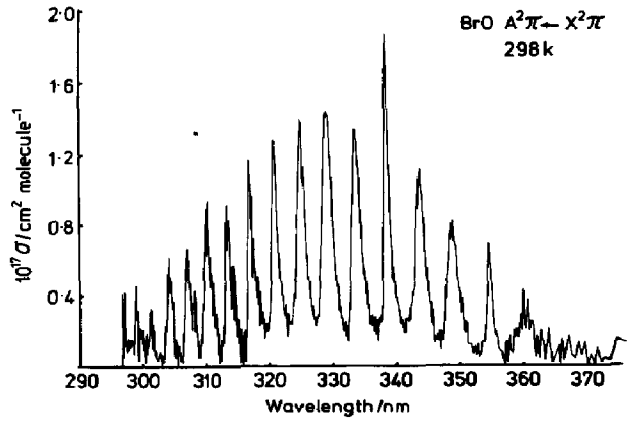

Fig. 2. Absorption spectrum for BrO in the 295 - 375 nm wavelength region obtained from measurements of in-phase modulated absorption in the 0.33 Hz photolysis of Br_2–O_3 mixtures.

the A $^2\Pi(v' = 7) \leftarrow$ X $^2\Pi(v'' = 0)$ transition and the bands illustrated in Fig. 2 cover the transitions $v' = 3 \leftarrow v'' = 0$ to $v' = 19 \leftarrow v'' = 0$. In the present work there were no clearly defined features at $\lambda > 361$ nm although there was an indication of additional absorption near 370 nm. The spectrum in Fig. 2 is plotted in terms of the absolute absorption cross section based on the measured absorption relative to that at 338.3 nm for which the absolute cross section was determined in the kinetic measurements described below.

3.2. Photolysis rate k_{11} of Br_2

The absolute cross section for absorption by BrO at 338.3 nm was determined from measurements of the kinetics of BrO in the photolysis of Br_2–O_3 mixtures using broad band visible radiation in the region 375 - 700 nm. Measurements of σ require a knowledge of the photochemical production rate of BrO. In this system atomic bromine is produced by photolysis of molecular Br_2 and BrO is formed rapidly by the reaction of Br with O_3. Calculation of the overlap of the fluorescent lamps with the O_3 absorption in the Chappuis bands showed that light absorption by O_3 was only 2% of that of Br_2 under typical experimental conditions. The rate of photodissociation of Br_2 was obtained from observation of the rate of photolytic decay of Br_2 in the presence of excess formaldehyde and O_2 when the following reactions are expected to occur:

$$Br_2 + h\nu \rightarrow 2Br \quad (11)$$

$$Br + HCHO \rightarrow HBr + CHO \quad (12)$$

$$CHO + O_2 \rightarrow HO_2 + CO \quad (13)$$

$$HO_2 + HO_2 \rightarrow H_2O_2 + O_2 \quad (14)$$

$$HO_2 + HCHO \rightarrow \text{products} \quad (15)$$

The rapid rate of reaction (12) ($k_{12} = 1.8 \times 10^{-12}$ cm^3 molecule^{-1} s^{-1} at 298 K [12, 13]) ensures efficient conversion of Br, produced in the photodissociation of Br_2 to HBr, which does not photolyse in the visible–near-UV region. The rate of decay of Br_2 is therefore a measure of the photolysis rate k_{11}.

The Br_2 concentration was monitored by absorption at 414 nm ($\sigma(Br_2) = 6.2 \times 10^{-19}$ cm^2 molecule^{-1}) and the photolysis rates were measured at 303, 325 and 348 K. Figure 3 shows logarithmic decay curves for Br_2 using one, two and three photolysis lamps with a modulation period of 1 s and initial concentrations of 1×10^{15} molecules Br_2 cm^{-3}, 1.5×10^{16} molecules HCHO cm^{-3} and 1.2×10^{18} molecules O_2 cm^{-3} diluted in 1 atm of nitrogen. The decay was linear up to 50% decomposition of Br_2 but at higher conversions the Br_2 decay slowed, presumably because of the regeneration of Br_2 by unknown secondary reactions. A heterogeneous reaction between the products H_2O_2 and HBr could account for this observation. The first-order rate coefficients k_d were determined from the slope in the linear region and the corresponding photodissociation rates ($k_{11} = 2k_d$)

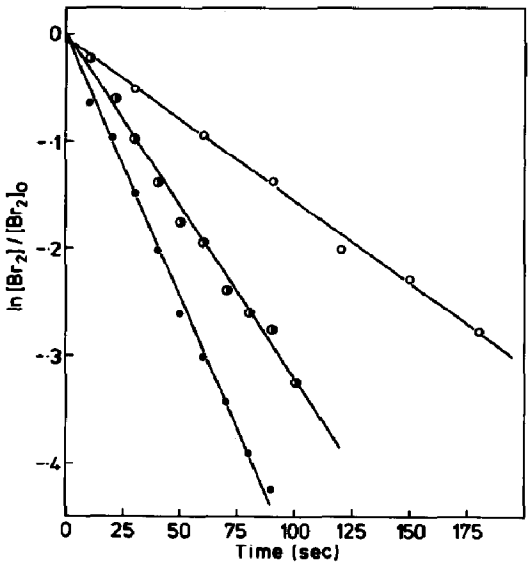

Fig. 3. Plot of $\ln([Br_2]/[Br_2]_0)$ *vs.* time for the decay of Br_2 in the photolysis of Br_2–HCHO–O_2 mixtures at 303 K: ○, one lamp; ⊕, two lamps; ●, three lamps.

were calculated. The values of k_{11} increased linearly with the number of lamps indicating good homogeneity of light intensity. The average value was $k_{11} = 3.5 \times 10^{-3}$ s^{-1} per lamp. The light intensity was also monitored photoelectrically so that fluctuations in intensity could be accounted for in subsequent experiments. There was no significant effect of temperature on the Br_2 photodissociation.

3.3. Quantum yield for Br_2-photosensitized decomposition of O_3

Mixtures of $(5 - 15) \times 10^{14}$ molecules Br_2 cm^{-3}, $(6.7 - 15.0) \times 10^{14}$ molecules O_3 cm^{-3} and 1.2×10^{18} molecules O_2 cm^{-3} diluted in 1 atm of nitrogen were photolysed with visible light (modulation period, 1 s) and the O_3 decay was followed by absorption at 280 nm ($\sigma(O_3) = 3.95 \times 10^{-18}$ cm^2 $molecule^{-1}$).

In a typical experiment the decay of O_3 was zero order in $[O_3]$ up to about 85% decomposition when the rate slowed down. The rates $-d[O_3]/dt$ were determined from the slopes of the linear portion of the decay curve and the quantum yields Φ were obtained from the ratio of these rates to the corresponding photodissociation rate, *i.e.* $0.5k_a[Br_2]$.

Table 1 shows a summary of the quantum yield data. The values given are mean values at each temperature obtained from experiments with varying Br_2 concentration and light intensity. No significant effect of these variables on $\Phi(-O_3)$ was observed. Although the amount of data collected was not large, it is clear that Φ increases with temperature. The values of Φ in excess of 2 indicate a chain reaction for O_3 decay in which the propagation rate increases with temperature relative to termination. The value of Φ at 303 K, *i.e.* 12.8 ± 2.0, is very similar to the limiting value $\Phi \approx 13$ for $[Br_2] > 2.0 \times$

TABLE 1

Quantum yields for the Br_2-photosensitized decomposition of O_3

Temperature (K)	Φ[a]	α[b]	k_4/k_5
277.5	9.1 ± 1.3 (3)	0.78 ± 0.03	3.50
303	12.8 ± 2.0 (9)	0.84 ± 0.03	5.25
325	14.5 ± 0.9 (4)	0.86 ± 0.01	6.14
348	16.6 ± 1.0 (3)	0.88 ± 0.01	7.30

[a] The number of experiments is given in parentheses.
[b] $\alpha = k_4/(k_4 + k_5)$ determined from $\Phi = 2/(1 - \alpha)$.

10^{17} molecules cm^{-3} and $[O_2] > 0.5$ atm observed in the more extensive study by Jaffe and Mainquist [9]. However, they observed higher values of Φ at the $[Br_2]$ and $[O_2]$ concentrations used in the present study and the temperature dependence of Φ determined by them was smaller. The quantitative agreement at 303 K may therefore be fortuitous.

3.4. Kinetics of the reaction BrO + BrO → Br_2 + O_2 (reaction (5))

The kinetics of reaction (5) were investigated by observation of the rise to steady state and subsequent decay of BrO radicals, monitored by absorption at 338.3 nm, in the photolysis of Br_2–O_3–O_2–N_2 mixtures. In this system BrO is produced and removed in the following reaction sequence:

$$Br_2 + h\nu \rightarrow Br + Br \quad (11)$$

$$Br + O_3 \rightarrow BrO + O_2 \quad (1)$$

$$BrO + BrO \rightarrow 2Br + O_2 \quad (4)$$

$$BrO + BrO \rightarrow Br_2 + O_2 \quad (5)$$

In view of the rapid rate of reaction (1) when O_3 is present in excess ($k_1 = 1.2 \times 10^{-12}$ cm^3 $molecule^{-1}$ s^{-1}) [14], net removal of BrO only occurs via reaction (5). The alternative pathway producing Br (reaction (4)) leads to regeneration of BrO via reaction (1) on a time scale of about 1 ms, *i.e.* much shorter than that for the overall decay of BrO which is about 100 ms.

Reaction mixtures containing typically 1×10^{15} molecules O_3 cm^{-3}, 1×10^{15} molecules Br_2 cm^{-3} and 2×10^{18} molecules O_2 cm^{-3} diluted in 1 atm of nitrogen were passed through the reaction vessel and absorption measurements were made under steady state flow conditions with modulation periods of 6 or 8 s and an averaging time of about 15 min. The residence time in the cell was 40 s.

Figure 4 shows a typical absorption–time profile obtained during the photolysis cycle as recorded on the multichannel detector. During the light-on period the BrO absorption rises rapidly to a steady state value and declines to a low value at the end of the dark period.

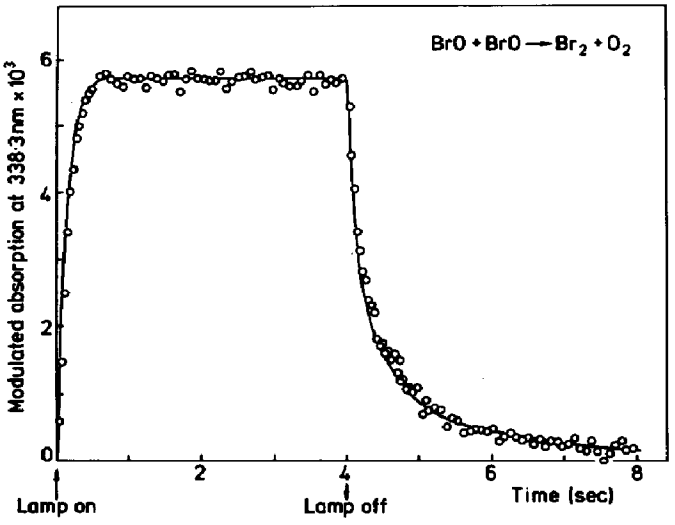

Fig. 4. Absorption–time profile for BrO during the square-wave-modulated photolysis cycle (averaging time, 600 s; $[Br_2] = 1.41 \times 10^{15}$ molecules cm^{-3}; $[O_3] = 1.68 \times 10^{15}$ molecules cm^{-3}; two-lamp photolysis): ——, computed using $k_5 = 7.1 \times 10^{-13}$ cm^3 $molecule^{-1}$ s^{-1} and $\sigma = 1.86 \times 10^{-17}$ cm^2 $molecule^{-1}$.

If it is assumed that the rate of removal of BrO by flow out of the cell is small compared with reaction (5), the time dependence of BrO is described by the following second-order rate equations:

$$\text{lamp on} \qquad \frac{d[BrO]}{dt} = 2B - 2k_5[BrO]^2 \tag{16}$$

$$\text{lamp off} \qquad \frac{d[BrO]}{dt} = -2k_5[BrO]^2 \tag{17}$$

where $2B$ is the rate of production of BrO radicals by photolysis of Br_2, *i.e.* $2k_{11}[Br_2]$.

It is clear from Fig. 4 that the steady state solution of eqn. (16) is applicable throughout most of the lamp-on period:

$$A_{SS} = \sigma l[BrO]_{SS} = \sigma l\left(\frac{B}{k_5}\right)^{1/2} \tag{18}$$

where A_{SS} is the steady state absorption due to BrO. It should be noted that the apparent steady state absorption in Fig. 4 will be slightly lower than the true value because only the change in absorbance is detected and, since the photolysis period is finite, a small residual concentration of BrO remains at the end of a cycle. For the conditions in Fig. 4 the residual BrO is about 2% of the maximum value and so the error introduced in using eqn. (18) for example for the determination of $k^{1/2}/\sigma$ directly from the experimental data is small.

Figure 5 shows a plot of the steady state absorption due to BrO as a function of the square root of the BrO production rate. The plot is linear in

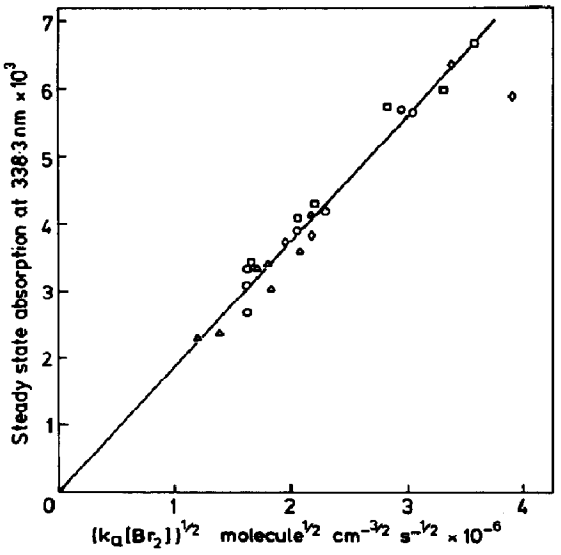

Fig. 5. Plot of the steady state absorption of BrO at 338.3 nm against the quantity $(k_a[Br_2])^{1/2}$ ($k_a = k_{11}$ × number of lamps): ◇, 278 K; ○, 303 K; □, 325 K; △, 348 K.

accord with eqn. (18) and the slope gives a mean value of $k^{1/2}/\sigma = (4.65 \pm 1.02) \times 10^{10}$ cm$^{-1/2}$ molecule$^{+1/2}$ s$^{-1/2}$.

Integration of eqns. (16) and (17) gives the following expressions for the half-times for rise to and fall from the steady state, *i.e.*

$$t_{1/2}(\text{rise}) = \frac{\ln 3}{4(Bk_5)^{1/2}} \tag{19}$$

$$t_{1/2}(\text{fall}) = \frac{1}{2(Bk_5)^{1/2}} \tag{20}$$

In Fig. 4 the ratio of the rise half-time (110 ms) to the fall half-time (210 ms) is about 0.5 as required for second-order kinetic behaviour. With a knowledge of B, k_5 can be evaluated directly from eqns. (19) and (20); the error introduced from the neglect of residual BrO is small in this case. The data give

k(rise time) = 6.7×10^{-13} molecules cm^{-3} s^{-1}

k(fall time) = 6.1×10^{-13} molecules cm^{-3} s^{-1}

A more accurate determination of the second-order rate coefficient for the decay of BrO in the dark period can in principle be made using the integrated form of eqn. (17):

$$\frac{1}{[\text{BrO}]_t} - \frac{1}{[\text{BrO}]_0} = 2k_5 t \tag{21}$$

However, in this analysis relatively large errors can be introduced if residual BrO is not taken into account. Thus a plot of (absorption)$^{-1}$ *versus* t showed distinct curvature at longer decay times when raw data such as those in Fig. 4 were used.

For modulated photolysis the residual absorption at the end of the cycle can be derived analytically but is a complex function of B, σ, k and τ, *i.e.* [15]

$$[BrO]_0 = \sigma l \left(\frac{B}{4k_5}\right)^{1/2} \{-C \pm (C^2 + 4D)\}$$

where $C = \mu \tanh \mu/(\mu + \tanh \mu)$, $D = C/\mu$ and $\mu = \tau(Bk_5)^{1/2}$.

Data analysis using eqn. (21) was carried out by a trial-and-error estimate of a value for the residual absorption which gave a linear plot for the {total absorption (observed + residual)}$^{-1}$ *versus* time over the entire decay curve. Such a plot is shown in Fig. 6 for the data from Fig. 4 with a residual absorption of 1.2×10^{-4}, *i.e.* 2.1% of the steady state absorption added to the observed values. The slope of the plot gives the quantity $k/\sigma = 3.57 \times 10^{-4}$ cm s^{-1} which, combined with the value of $\sigma/k^{1/2} = 2.17 \times 10^{-11}$ cm$^{1/2}$ molecule$^{-1/2}$ s$^{1/2}$ obtained from this experiment using eqn. (18) gives $k_5 = 6.0 \times 10^{-13}$ cm^3 molecule^{-1} s^{-1} and $\sigma = 1.68 \times 10^{-17}$ cm^2 molecule^{-1}. This analysis is only valid if the kinetics are truly second order. The tests according to eqns. (18) - (20) give a good indication of the kinetics but do not reveal a small first-order component. The presence of a first-order component would result in an overestimation of the residual absorption and the value of k/σ from the plot of eqn. (21) would be underestimated.

Table 2 gives a summary of the values of k_5 and σ obtained from treatment in the above fashion of the data from all the experiments at the four temperatures employed. Considering the uncertainty limits, which represent twice the standard deviation from the mean of the individual experiments, there was no significant temperature dependence of k_5 or σ over the range 277.5 - 348 K. The mean values of k and σ over this range obtained in the present experiments are

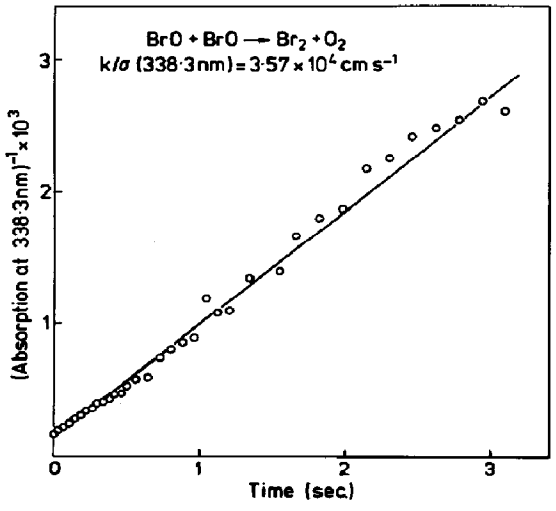

Fig. 6. Plot of the corrected reciprocal absorption *vs.* time for the BrO decay illustrated in Fig. 4 (see text for correction procedure).

TABLE 2

Rate coefficients and absorption cross sections from BrO kinetics

Temperature (K)	k_5/σ[a] ($\times 10^4$ cm s^{-1})	k_5 ($\times 10^{-13}$ cm^3 $molecule^{-1}$ s^{-1})	σ[b] ($\times 10^{-17}$ cm^2 $molecule^{-1}$)
277.5	4.20 ± 0.50 (7)	7.4 ± 1.6	1.7 ± 0.3
303.0	3.75 ± 0.40 (11)	6.9 ± 1.4	1.8 ± 0.3
325.0	3.50 ± 0.40 (6)	6.0 ± 1.0	1.7 ± 0.2
348.0	3.74 ± 0.40 (7)	6.3 ± 1.0	1.7 ± 0.2

[a] The number of individual experiments is given in parentheses.
[b] At 338.3 nm.

$$k_5 = (6.6 \pm 2.0) \times 10^{-13} \text{ cm}^3 \text{ molecule}^{-1} \text{ s}^{-1} \qquad (278 - 348 \text{ K})$$

$$\sigma = (1.75 \pm 0.35) \times 10^{-17} \text{ cm}^2 \text{ molecule}^{-1} \qquad (338.3 \text{ nm})$$

The uncertainty limits are estimated to include both experimental errors and possible systematic errors in the data treatment.

In order to check the validity of the data analysis described above, computer simulation of the modulation waveform for [BrO] absorption was performed. The Harwell program FACSIMILE [16] was employed to integrate the kinetic equations and generate absorption–time profiles for comparison with experiment. The unknown parameters k_5 and σ were varied to give the best fit using a non-linear least-squares routine. Simulation of the experiment illustrated in Fig. 4 was carried out using a mechanism involving reactions (1), (4), (5) and (11) with $k_4/(k_4 + k_5) = 0.84$. The values of k_5 and σ generated were $k_5 = 7.1^{+3.0}_{-2.5} \times 10^{-13}$ cm^3 $molecule^{-1}$ s^{-1} and $\sigma = (1.86 \pm 2.0) \times 10^{-17}$ cm^2 $molecule^{-1}$, and the corresponding curve is shown in Fig. 4. The higher values of k_5 and σ compared with those obtained by graphical analysis result in shorter rise and fall times than were actually observed, and this is reflected in the rather large error limits on the fitted value of k_5. The differences in detail are not considered sufficient to invalidate the analytical treatment of the data. They probably arise from inadequacies in the non-linear least-squares fitting procedure which needs to be explored further.

4. Discussion

4.1. Absorption cross section of BrO

Table 3 shows the available data for the absorption cross section for BrO in the 7–0 band near 338.5 nm. The values are not strictly comparable since they were determined at different spectral resolutions and in the case of the results of Sander and Watson [4] were slightly off the band head at 339.0 nm. In the present work it was found that BrO absorption at

TABLE 3

Absorption cross section for BrO in the 7–0 band of the A $^2\Pi \leftarrow$ X $^2\Pi$ system near 338.3 nm

Reference	*Wavelength (spectral resolution)* (nm)	σ ($\times 10^{-18}$ cm^2 molecule^{-1})
[2][a]	338.3 (not given)	4.7 ± 0.4
[5][b]	338.3 (1.0)	8.0 ± 0.9
[4][c]	339.0 (0.1)	11 ± 1.4
This work	338.3 (0.22)	18 ± 2.0

[a] Flash photolysis of Br_2–OClO mixtures; [BrO] at $t = 0$ equated to [ClO] at $t = 0$.
[b] Discharge flow; BrO produced by Br + O_3 reaction; [BrO] determined from reaction stoichiometry with correction for BrO decay.
[c] Flash photolysis of Br_2–O_3 mixtures; the measured amount of O_3 was completely converted to BrO; the initial absorption was determined by a short extrapolation from the BrO decay.

339.0 nm with a spectral slit width of 0.11 nm was a factor of 0.50 ± 0.05 lower than the standard conditions used for our measurements (338.3 nm with a slit width of 0.22 nm). Thus a value of $\sigma = (9.0 \pm 1.5) \times 10^{-18}$ cm^3 molecule at 339 nm is implied in good agreement with that of Sander and Watson [4]. Measurements at 338.3 nm were not made at 1.0 nm resolution as was used by Clyne and Cruse [5] but at 0.55 nm the BrO absorption had decreased to 85% of the standard value. Therefore σ would be expected to be considerably lower than 1.5×10^{-18} cm^2 molecule^{-1} at 1.0 nm resolution. The earlier value of Basco and Dogra [2] is based on an incorrect interpretation of their data [6] and is open to doubt. The measurement of Sander and Watson [4] is least subject to error since it is totally independent of the measured rate coefficient for BrO decay whereas in the present work and that of Clyne and Cruse the derived values of the rate coefficients and σ are coupled. The agreement between the present value and that measured independently of k_4 or k_5 lends confidence to the use of our value to determine the absolute cross sections over the wavelength region 375 - 296 nm from the values obtained relative to that at 338.3 nm. The absolute values are plotted in Fig. 2 and average values for 10 nm wavelength intervals are listed in Table 4. The absorption cross section determined in the present study was independent of temperature over the range 278 - 348 K. Sander and Watson [4] observed a significant temperature dependence: σ(339 nm) increased from 9.6×10^{-18} cm^2 molecule^{-1} at 388 K to 1.56×10^{-17} cm^2 molecule^{-1} at 223 K. The precision of our measurements was probably not sufficient to detect this effect over the smaller temperature range used in this study.

4.2. Rate coefficient for the reaction BrO + BrO → products

A summary of the data for k_4 and k_5 at room temperature is given in Table 5. The only previous direct determination of k_5 is that of Sander and

TABLE 4

Averaged absorption cross sections and solar photolysis rates of BrO

Wavelength range (nm)	*Average* σ ($\times 10^{-18}$ cm^2 molecule^{-1})	$j_\lambda = \sigma_\lambda I_\lambda$[a] ($\times 10^{-3}$ s^{-1})
300 - 305	2.00	0.05
305 - 310	2.59	0.27
310 - 315	4.54	1.17
315 - 320	3.91	1.46
320 - 325	6.00	2.88
325 - 330	7.53	5.28
330 - 335	6.28	4.71
335 - 340	5.89	4.40
340 - 345	5.15	4.17
345 - 350	3.99	3.23
350 - 355	2.28	2.10
355 - 360	1.72	1.47
360 - 365	1.61	1.53
365 - 370	0.92	1.08
370 - 375	0.51	0.54
		$\Sigma = 34.34$

[a] For a zenith angle of 30°.

TABLE 5

Rate coefficients for the reaction BrO + BrO → products at room temperature

Reference	k_5[a] ($\times 10^{-13}$ cm^3 molecule^{-1} s^{-1})	$k_4 + k_5$ ($\times 10^{-12}$ cm^3 molecule^{-1} s^{-1})
[2]	—	1.03 ± 0.13[b]
[5]	(8.32)	5.2 ± 0.07[c]
[6]	(5.07)	3.17 ± 0.67[d]
[4]	(4.1 ± 2.0)[e] 3.5 ± 0.7	2.17 ± 0.68
This work	6.6 ± 2.0	(4.1 ± 1.5)

[a] The values in parentheses were calculated using $k_5/(k_4 + k_5) = 0.84$.
[b] Value uncertain because of the doubtful value of σ used to calculate k_4.
[c] Error larger than indicated because of the uncertainty in σ.
[d] $k_4 + k_5$ was determined by discharge flow–mass spectrometry detection of BrO and hence is independent of σ.
[e] Direct and indirect values of k_5 (see text).

Watson [4]. The flash photolysis–UV absorption technique was employed to determine k_5/σ for the second-order decay of BrO in the presence of excess O_3. The results gave $k_5 = (3.46 \pm 0.68) \times 10^{-13}$ cm^3 molecule^{-1} s^{-1} at 298 K using $\sigma = 1.14 \times 10^{-17}$ cm^2 molecule^{-1} at 339.0 nm. Sander and Watson also reported an indirect determination of k_5 from the ratio $\alpha = k_4/(k_4 + k_5) = 0.84 \pm 0.03$ obtained from measurements of the number of O_3

molecules removed for each BrO molecule produced in the flash in the Br_2–excess O_3 system. By combining this result with their measured value of the overall rate coefficient for BrO + BrO with respect to all products, *i.e.* $k_4 + k_5 = (2.17 \pm 0.68) \times 10^{-12}$ cm^3 molecule^{-1} s^{-1}, they obtained $k_5 = (4.12 \pm 1.99) \times 10^{-13}$ cm^3 molecule^{-1} s^{-1}. Both values are considerably lower than that found in the present work.

Independent support for the value of α comes from measurements of the quantum yield for O_3 decomposition in the Br_2–O_3 photolysis system. For a simple scheme involving reactions (11), (1), (4) and (5) it can readily be shown that

$$\Phi = \frac{2}{1 - \alpha}$$

The present study gave $\Phi \approx 12.8$ at 303 K and Jaffe and Mainquist [9] obtained $\Phi \approx 13$ at 298 K, yielding $\alpha = 0.84$. The values at other temperatures are summarized in Table 1.

The value of $\alpha = 0.84 \pm 0.03$ at 298 K can be combined with the value of k_5 determined in this work to give $k_4 + k_5 = (4.1 \pm 1.5) \times 10^{-12}$ cm^3 molecule^{-1} s^{-1}. The CODATA [17] recommended value is a mean of the determinations of Watson and Clyne [6] and Sander and Watson [4], *i.e.* 2.8×10^{-12} cm^3 molecule^{-1} s^{-1}, the higher value obtained by Clyne and Cruse [5] being rejected on account of the uncertainty in the value of σ in their study. The preferred value is significantly lower than the value obtained at 303 K in the present work. Our results do not therefore resolve the discrepancies in the values of the overall rate constant for the BrO + BrO reaction at 298 K.

A temperature-independent value of k_5 has been reported in the present work but there is an indication of a slight negative temperature dependence. A least-squares treatment of the data in Table 2 according to the Arrhenius equation gave

$$k_5 = 2.9^{+2.8}_{-1.4} \times 10^{-13} \exp\left(\frac{259 \pm 208}{T}\right) \text{ cm}^3 \text{ molecule}^{-1} \text{ s}^{-1}$$

Previous studies of the BrO + BrO reaction have only provided information on the temperature dependence of the overall rate $k_4 + k_5$.

Although the results of these studies all concur that the overall rate coefficient $k_4 + k_5$ shows only a small temperature dependence, the reported values for E/R (—244 ± 100 K and 450 ± 300 K) are of opposite sign. Furthermore Brown and Burns [3] have reported a positive temperature dependence with distinct non-Arrhenius behaviour for $(k_4 + k_5)/\sigma$ over the range 300 - 700 K. Part of the disagreement in detail could arise from the temperature dependence of σ, which may well extend to higher temperatures.

The temperature dependence of the branching ratio k_4/k_5 can be obtained from analysis of the temperature dependence of the O_3 decay quantum yield if the simple mechanism involving reactions (11), (2), (4) and (5) applies in this system. The data in Table 1 give

$$\frac{k_4}{k_5} = 130 \exp\left(-\frac{992 \pm 210}{T}\right)$$

The results of Jaffe and Mainquist [9] give a considerably lower temperature dependence:

$$\frac{k_4}{k_5} = 14.6 \exp\left(-\frac{276 \pm 35}{T}\right)$$

If we take a mean of these two temperature dependences $(E_4 - E_5)/R = 634 \pm 360$ K and the A factors $A_4/A_5 = 40.7$ together with the Arrhenius expression obtained in the present work for k_5 we obtain

$$k_4 = 1.2 \times 10^{-11} \exp\left(-\frac{375 \pm 415}{T}\right) \text{ cm}^3 \text{ molecule}^{-1} \text{ s}^{-1}$$

Thus these results support a slight positive activation energy for the radical formation channel in the BrO + BrO reaction as reported by Clyne and Cruse [5] and Brown and Burns [3]. However, the small negative temperature coefficient for $k_4 + k_5$ observed by Sander and Watson [4] is more in line with other reactions between small radicals. If the latter work is correct then the present results for k_5 imply that the temperature dependence of Φ arises from reactions other than the branching and termination channels in the BrO + BrO reaction.

A possible explanation of the effect of O_2 and the large temperature dependence of Φ is the involvement of electronically excited O_2 molecules. Sufficient energy is available in reaction (1) to produce the $^1\Delta$ state of O_2 and in reaction (5) to produce either the $^1\Delta$ or the $^1\Sigma$ states. Both singlet O_2 species react with O_3:

$$O_2(^1\Delta \text{ or } ^1\Sigma) + O_3 \rightarrow O(^3P) + 2O_2 \qquad (22)$$

At high $[O_2]$ the $O(^3P)$ species would be expected mainly to re-form O_3 by reaction (10), but any reaction occurring between $O(^3P)$ and Br_2 or BrO would lead to enhanced O_3 decay. Reaction (22) has an activation energy of 23.6 kJ mol^{-1} for $O_2(^1\Delta)$, and therefore the competition between reaction (22) and the slow quenching of $O_2(^1\Delta)$, *e.g.* by O_2 or at the vessel walls, could be temperature dependent.

4.3. Photolysis rate for BrO in the atmosphere

The solar photolysis rate J(BrO) of BrO can be calculated from the integrated overlap of the absorption spectrum of BrO and the intensity spectrum of solar radiation in the appropriate wavelength region, *i.e.*

$$J(\text{BrO}) = \sum_{\lambda} I_\lambda \alpha_\lambda$$

where σ and I are average values of the cross section and the intensity over the wavelength interval chosen for the summation. Table 4 gives a tabulation of the appropriate values of I and σ averaged over 5 nm intervals for a solar zenith angle of 30° using σ values from this work and ground level intensity data from Peterson [18] which are based on observation. The resolution

should be adequate to give a sufficiently accurate value of the integrated J value even for the strongly structured BrO absorption. The value obtained is $3.4_3 \times 10^{-2}$ s^{-1}, implying a BrO lifetime with respect to photolysis of 20 s at this sun angle at the Earth's surface. Since most of the absorption takes place at wavelengths greater than 320 nm which are not strongly attenuated by the atmosphere, this photolytic rate will be almost constant with altitude at a given solar zenith angle.

According to Durie and Ramsay [1] dissociation from the A $^2\Pi$ upper state of the halogen monoxides yields atomic oxygen in the excited state:

$$BrO(A\ ^2\Pi) \rightarrow Br(^2P_{3/2}) + O(^1D)$$

Since the A $\leftarrow$ X transition is extensively predissociated, absorption of light leads to efficient dissociation of BrO, thereby increasing the ratio [Br]/[BrO] in the atmosphere. The other reactions which are also important for conversion of BrO to Br in the atmosphere are

$$BrO + NO \rightarrow Br + NO_2 \qquad k = 2.8 \times 10^{-11}\ cm^3\ molecule^{-1}\ s^{-1}$$

$$BrO + O \rightarrow Br + O_2 \qquad k = 3 \times 10^{-11}\ cm^3\ molecule^{-1}\ s^{-1}$$

$$BrO + ClO \rightarrow Br + ClO_2 \qquad k = 1.34 \times 10^{-11}\ cm^3\ molecule^{-1}\ s^{-1}$$

If average values of the mixing ratios of NO, O and ClO taken from one-dimensional model calculations for an altitude of 25 km and a temperature of 222 K (10^{-9}, 2.5×10^{-11} and 10^{-10} respectively [19]) are used, the effective rates of these reactions are 2.3×10^{-2} s^{-1}, 0.05×10^{-2} s^{-1} and 0.1×10^{-2} s^{-1} respectively. Therefore photolysis is the major route for conversion of BrO to Br in the middle stratosphere where the catalytic destruction of O_3 by BrO_x reactions is potentially important. However, as has been shown by Watson *et al.* [8] the magnitude of the effect of BrO_x on O_3 is not particularly sensitive to the value of the [Br]/[BrO] ratio. This arises because BrO is the major bromine-containing species at these altitudes and quite large changes in the above ratio only result in modest changes to the fraction of the total bromine which is present as BrO. Since the rate-determining steps for catalytic destruction of O_3 all involve BrO, the fraction [BrO]/[total BrO_x] is the key quantity determining the efficiency of ozone depletion from bromine species.

Acknowledgments

This work was sponsored jointly by the U.K. Department of the Environment and the European Economic Community Environment Programme under Contract ENV-454-UK.

References

1 R. A. Durie and D. A. Ramsay, *Can. J. Phys.*, *36* (1958) 35.
2 N. Basco and S. D. Dogra, *Proc. R. Soc. London, Ser. A*, *323* (1971) 1.
3 J. Brown and G. Burns, *Can. J. Chem.*, *48* (1970) 3487.
4 S. P. Sander and R. T. Watson, *J. Phys. Chem.*, to be published.
5 M. A. A. Clyne and H. W. Cruse, *Trans. Faraday Soc.*, *66* (1970) 2214.
6 M. A. A. Clyne and R. T. Watson, *J. Chem. Soc., Faraday Trans. I*, *71* (1975) 336.
7 S. C. Wofsy, M. B. McElroy and Y. L. Yung, *Geophys. Res. Lett.*, *2* (1975) 215.
8 R. T. Watson, S. P. Sander and Y. L. Yung, *J. Phys. Chem.*, *83* (1979) 2936.
9 S. Jaffe and W. K. Mainquist, *J. Phys. Chem.*, *84* (1980) 3277.
10 R. A. Cox, R. G. Derwent, A. E. J. Eggleton and H. J. Reid, *J. Chem. Soc., Faraday Trans. I*, *75* (1979) 1648.
11 M. Barnett, E. A. Cohen and D. A. Ramsay, *Can. J. Phys.*, to be published.
12 G. Poulet, G. Laverdet and G. Le Bras, *J. Phys. Chem.*, *85* (1981) 1892.
13 D. F. Nava, J. V. Michael and L. J. Stief, *J. Phys. Chem.*, *85* (1981) 1896.
14 M. T. Leu and W. B. DeMore, *Chem. Phys. Lett.*, *48* (1977) 317.
15 G. E. McGraw and H. S. Johnston, *Int. J. Chem. Kinet.*, *1* (1969) 89.
16 E. M. Chance, A. R. Curtis, I. P. Johns and C. R. Kirby, *AERE Rep. R 8775*, 1977 (Atomic Energy Research Establishment, Harwell).
17 D. L. Baulch, R. A. Cox, R. F. Hampson, Jr., J. A. Kerr, J. Troe and R. T. Watson, *J. Phys. Chem. Ref. Data*, *9* (1980) 295.
18 J. P. Peterson, *EPA Rep. 600/4-76-025*, June 1976 (U.S. Environment Protection Agency, Research Triangle Park, NC).
19 R. D. Hudson and E. I. Reed (eds.), The stratosphere — present and future, *NASA Rep. RP 1049*, 1979 (National Aeronautics and Space Administration).